Human Molecular Genetics, 2018, Vol. 27, No. 18 3165–3176

doi: 10.1093/hmg/ddy219
Advance Access Publication Date: 8 June 2018
Original Article

ORIGINAL ARTICLE

Ulk2 controls cortical excitatory–inhibitory balance via autophagic regulation of p62 and $GABA_A$ receptor trafficking in pyramidal neurons

Akiko Sumitomo[1], Hiroshi Yukitake[2], Kazuko Hirai[1], Kouta Horike[1], Keisho Ueta[1], Youjin Chung[2], Eiji Warabi[3], Toru Yanagawa[3], Shiho Kitaoka[4,5], Tomoyuki Furuyashiki[4,5], Shuh Narumiya[4], Tomoo Hirano[6], Minae Niwa[2], Etienne Sibille[7], Takatoshi Hikida[1], Takeshi Sakurai[1], Koko Ishizuka[2], Akira Sawa[2,*] and Toshifumi Tomoda[1,7,*]

[1]Department of Research and Drug Discovery, Medical Innovation Center, Kyoto University Graduate School of Medicine, Kyoto 606-8507, Japan, [2]Department of Psychiatry and Behavioral Sciences, Johns Hopkins University School of Medicine, Baltimore, MD 21287, USA, [3]Faculty of Medicine, University of Tsukuba, Tsukuba 305-8575, Japan, [4]CREST Project, Medical Innovation Center, Kyoto University Graduate School of Medicine, Kyoto 606-8507, Japan, [5]Department of Pharmacology, Kobe University Graduate School of Medicine, Hyogo 650-0017, Japan, [6]Department of Biophysics, Kyoto University Graduate School of Science, Kyoto 606-8502, Japan and [7]Campbell Family Mental Health Research Institute, Centre for Addiction and Mental Health, University of Toronto, Toronto, ON M5T 1R8, Canada

*To whom correspondence should be addressed at: Department of Psychiatry and Behavioral Sciences, Johns Hopkins University School of Medicine, Baltimore, MD 21287, USA. Tel: +1 4109554726; Email: asawa1@jhmi.edu (A.S.); Campbell Family Mental Health Research Institute, Centre for Addiction and Mental Health, University of Toronto, Toronto, ON M5T 1R8, Canada. Tel: +1 4165358501; Email: ttomoda1@gmail.com (T.T.)

Abstract

Autophagy plays an essential role in intracellular degradation and maintenance of cellular homeostasis in all cells, including neurons. Although a recent study reported a copy number variation of *Ulk2*, a gene essential for initiating autophagy, associated with a case of schizophrenia (SZ), it remains to be studied whether *Ulk2* dysfunction could underlie the pathophysiology of the disease. Here we show that *Ulk2* heterozygous ($Ulk2^{+/-}$) mice have upregulated expression of sequestosome-1/p62, an autophagy-associated stress response protein, predominantly in pyramidal neurons of the prefrontal cortex (PFC), and exhibit behavioral deficits associated with the PFC functions, including attenuated sensorimotor gating and impaired cognition. $Ulk2^{+/-}$ neurons showed imbalanced excitatory–inhibitory neurotransmission, due in part to selective down-modulation of gamma-aminobutyric acid $(GABA)_A$ receptor surface expression in pyramidal neurons. Genetically reducing *p62* gene dosage or suppressing p62 protein levels with an autophagy-inducing agent restored the $GABA_A$ receptor surface expression and rescued the behavioral deficits in $Ulk2^{+/-}$ mice. Moreover, expressing a short peptide that specifically interferes with the interaction of p62 and $GABA_A$ receptor-associated protein, a protein that regulates endocytic trafficking of $GABA_A$ receptors, also restored the $GABA_A$ receptor surface expression and rescued the behavioral deficits in $Ulk2^{+/-}$ mice.

Received: January 26, 2018. **Revised:** May 22, 2018. **Accepted:** June 4, 2018

Thus, the current study reveals a novel mechanism linking deregulated autophagy to functional disturbances of the nervous system relevant to SZ, through regulation of $GABA_A$ receptor surface presentation in pyramidal neurons.

Introduction

Macroautophagy (hereafter referred to as autophagy) is a specialized membrane trafficking machinery and a major cellular recycling system responsible for degrading old proteins and damaged organelles, which ultimately serve as resources to generate new proteins and energy, and thus critical to the maintenance of cellular homeostasis (1). In response to a range of cellular stresses (e.g. depletion of nutrients and energy, misfolded protein accumulation and oxidative stress), autophagy is activated to mitigate such stresses via activation of ULK1/ULK2/ATG1, serine/threonine protein kinases critical to the regulation of autophagy induction. Subsequently, microtubule-associated protein light chain 3 (LC3)-positive autophagosomes are formed to enwrap the proteins and organelles that are selectively labeled with sequestosome-1/p62, an autophagy-related stress response protein, and then trafficked to fuse with lysosomes for degradation.

A role of autophagy in the nervous system was previously shown in nervous system-specific *Atg5* and *Atg7* conditional knockout (cKO) mice, which exhibit progressive neuronal death, accompanied by accumulation of abnormal cytosolic proteins and formation of p62-positive inclusions in neurons (2–4). These results suggested that continuous quality control of diffuse cytosolic proteins via basal autophagy is important for neuronal functions. Subsequently, we and others provided evidence that autophagy regulates synapse morphogenesis and function, using a series of autophagy-deficient mutants in *Drosophila melanogaster*, which demonstrate diminished size and number of synaptic boutons and a decrease in evoked neurotransmitter release (5–8). Meanwhile, ULK1/ULK2/ATG1 regulate endocytic trafficking of neuronal cargoes through association with a synaptic protein SynGAP (9), and also regulate trafficking of synaptic vesicles via association with additional neuronal proteins, such as Unc-76/FEZ1 and synaptotagmin-1 (5). In accordance with these observations, dopaminergic neuron-specific *Atg7*-cKO mice showed a role of autophagy in presynaptic structure and neurotransmission, exhibiting enlarged striatal axon terminal profiles and abnormally increased dopamine release (10). It is thus possible that autophagy-mediated regulation of pre- or post-synaptic components via modulation of their trafficking could contribute to neural plasticity. However, questions remain as to: (i) whether neuronal autophagy is involved in higher brain functions, such as cognition; (ii) if so, which brain regions and neuronal cell types are most vulnerable to impaired autophagy, leading to specific behavioral outcomes and (iii) what are molecular mechanisms that account for such outcomes.

A recent study showed that mice doubly deficient for *Ulk1* and *Ulk2* in the nervous system have a slight increase in the levels of p62 protein, a key target molecule in autophagic protein degradation, without showing a sign of p62-positive inclusions (11). Likewise, mice deficient for *Ulk1* had increased levels of p62 protein expression in the prefrontal cortex (PFC) (12). Importantly, unlike the knockout of non-redundant autophagy genes such as *Atg5* and *Atg7* that display early postnatal death in mice and may possibly mask the underlying neural mechanisms, *Ulk1* and *Ulk2* have redundant roles in autophagy and mice singly deficient for either of these genes are viable with no overt deficits in overall physical conditions, such as life span, body weight and motor functions (12–15). Thus, we regard that perturbation of *Ulk1* and/or *Ulk2* will provide the best model to address the current questions. With this model, it is expected that we could address whether this pathway plays a causal role in neurobehavioral manifestation. In this regard, it is notable that the copy number variations (CNVs) of *ULK1/ULK2/ULK4* family member genes were recently reported to be enriched in schizophrenia (SZ) patients recruited in a genome-wide association study (odds ratio =6.77) (16).

In the present study, we set out to test whether *Ulk2* heterozygous ($Ulk2^{+/-}$) mice have signs of attenuated autophagy (i.e. elevated p62 expression) in certain regions or cell types within the brain, and addressed whether such changes can be linked to neurobehavioral outcomes. We hypothesized that elevated p62 levels have functional consequences on neurotransmission that could account for the observed behavioral deficits relevant to SZ.

Results

$Ulk2^{+/-}$ mice show elevated p62 protein levels in the PFC

As described above, changes in the expression of p62 protein have been reported in both *Ulk1* and *Ulk2* knockout mice (11,12). However, a question remains as to which brain regions and cells most robustly represent such changes. Thus, we first examined the expression of p62 protein in various brain regions of $Ulk2^{+/-}$ mice. The mutants had significantly elevated expression of p62 protein in the medial PFC (Fig. 1A and B; Supplementary Material, Fig. S1A and B), which occurred in Ca^{2+}/calmodulin-dependent protein kinase II (CaMKII)-positive pyramidal neurons, but not in the interneurons (Fig. 1A; Supplementary Material, Fig. S1B). This elevated p62 expression was seen in the PFC, but not in all other brain regions tested, including the visual cortex, nucleus accumbens, dorsal striatum, hippocampus and ventral tegmental area (Supplementary Material, Fig. S1A). Taken together, reduced expression of *Ulk2* affects cellular processes involving p62 protein, likely associated with autophagic homeostasis, in a neuronal cell-type preferential and a brain region-preferential manner.

$Ulk2^{+/-}$ mice show behavioral deficits associated with the PFC function

We then questioned whether and how the reduction in *Ulk2* affects the PFC-relevant behaviors, including sensorimotor gating (17) and cognitive flexibility (18). $Ulk2^{+/-}$ mice had impaired sensorimotor gating, showing lower levels of prepulse inhibition (PPI) of acoustic startle stimuli (Fig. 1C and D). To assess the PFC-dependent cognitive function, $Ulk2^{+/-}$ mice were tested in a rule shifting paradigm (19,20), in which mice were initially trained to associate food reward with a specific stimulus (i.e. either an odor or a digging medium) and subsequently evaluated for cognitive flexibility by changing the type of stimulus that predicts the reward (Fig. 1E). Although both $Ulk2^{+/-}$ and WT mice learned the association rule in a similar number of trials during the initial association phase of trials, $Ulk2^{+/-}$ mice were specifically impaired during the rule shifting phase of trials (Fig. 1F and G).

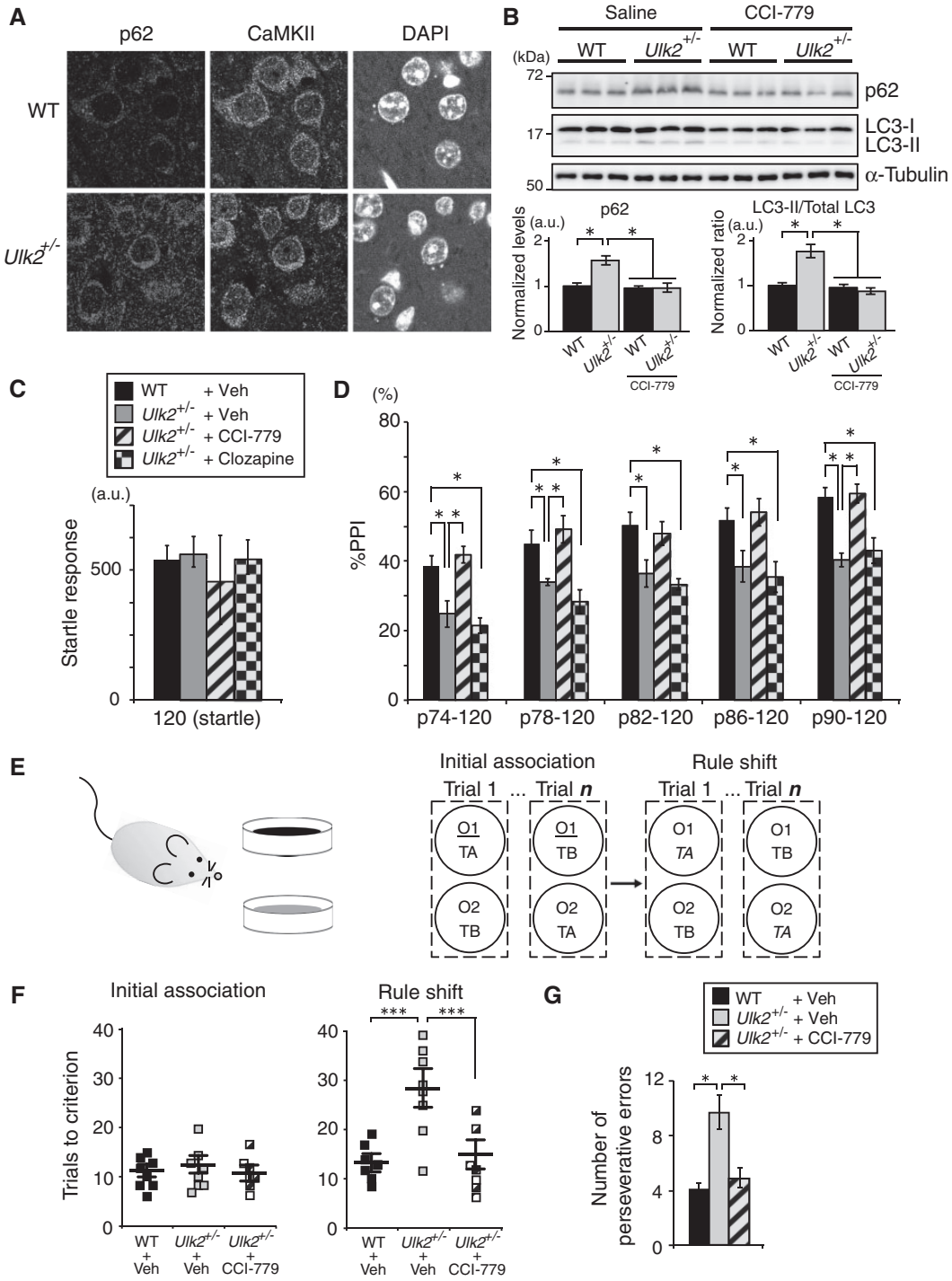

Figure 1. Upregulated p62 protein levels in pyramidal neurons of the PFC and PFC-associated behavioral deficits in *Ulk2*$^{+/-}$ mice. (**A**) Selective upregulation of p62 protein in CaMKII^{+} neurons in the PFC of *Ulk2*$^{+/-}$ mice. Scale bar, 10 μm. (**B**) Western blot of p62 and LC3 in the frontal cortex of *Ulk2*$^{+/-}$ mice chronically treated with saline or a rapamycin analog CCI-779. The expression levels were measured by densitometric analysis using ImageJ. Error bars indicate SEM. *P <0.05. (**C**, **D**) The amplitude of startle response (C) and the percentage of PPI (D) were evaluated for WT+saline (n=10), *Ulk2*$^{+/-}$+saline (n=10), *Ulk2*$^{+/-}$+CCI-779 (n=10) and *Ulk2*$^{+/-}$+clozapine (n=10). No significant difference in startle response [$F_{(3, 36)}$=0.9683, P=0.4183] (one-way ANOVA). Statistical significance for %PPI: $F_{(3, 36)}$=11.28, P <0.0001 (two-way ANOVA with repeated measures); *P <0.05 (Bonferroni post hoc test). (**E**) Schematic diagram of the rule shift assay. Upon rule shifting, the stimulus associated with food reward is changed from odor cue 1 (underlined) to texture cue A (italicized) in this diagram. (**F**) Numbers of trials to criterion during the initial association phase, as well as the rule shift phase of the assays, were scored for WT (n=8), *Ulk2*$^{+/-}$ (n=8) and *Ulk2*$^{+/-}$+CCI-779 (n=7). No significant difference during the initial association phase [$F_{(2, 20)}$=1.54, P=0.832]. Statistical significance during the rule-shift phase: $F_{(2, 20)}$=7.67, P<0.0001 (one-way ANOVA); ***P <0.001 (Bonferroni post hoc test). (**G**) Numbers of perseverative errors during the rule shift phase were scored. $F_{(2, 20)}$=4.83, P=0.024 (one-way ANOVA); *P <0.05 (Bonferroni post hoc test).

CaMKII-specific Ulk2$^{+/-}$ mice show behavioral deficits associated with the PFC function

We next investigated specific roles of neuronal subtypes in the observed phenotypes. Mice heterozygous for conditional *Ulk2* knockout allele were crossed with mice expressing either pan-specific Cre (EIIa-Cre), pyramidal neuron-specific Cre (CaMKII-Cre), or interneuron-specific Cre (Viaat-Cre) and PPI was measured. When *Ulk2* was ablated in an interneuron-specific manner, PPI was not affected (Supplementary Material, Fig. S1C–E). In contrast, pyramidal neuron-specific *Ulk2* ablation resulted in attenuated PPI (Supplementary Material, Fig. S1C, D and F). These data are in line with the notion that homeostatic deficits involving p62 accumulation in the CaMKII-positive pyramidal neurons underlie the PPI deficits in *Ulk2*$^{+/-}$ mice.

Reduced surface expression of $GABA_A$ receptors and imbalanced excitatory–inhibitory neurotransmission in *Ulk2*$^{+/-}$ pyramidal neurons

To further investigate molecular and cellular basis that may underlie these behavioral changes, electrophysiological properties of the cultured pyramidal neurons prepared from *Ulk2*$^{+/-}$ mice were examined. Typically, ∼80% of neurons in culture were CaMKII-positive pyramidal neurons, and ∼20% were glutamic acid decarboxylase 67 (GAD67)-positive interneurons under the culture condition, as confirmed by immunostaining performed after electrophysiological recording. Patch-clamp recording of *Ulk2*$^{+/-}$ pyramidal neurons revealed altered excitatory–inhibitory neurotransmission; the frequencies and amplitudes of miniature excitatory postsynaptic currents (mEPSC) were elevated, whereas the miniature inhibitory postsynaptic currents (mIPSC) amplitudes were downregulated, suggesting an excitatory-dominant state at the resting condition (Fig. 2A). Next, depolarization-induced increases in calcium $[Ca^{2+}]_i$ were measured in CaMKII-positive pyramidal neurons by transfecting GCaMP Ca^{2+} sensor probe in culture (Supplementary Material, Fig. S2). *Ulk2*$^{+/-}$ primary neurons showed higher levels of peak $\Delta F/F_0$ and slower rates of fluorescence decay than WT neurons (Fig. 2B). These data indicate higher excitability and lower responsiveness to inhibitory signals in *Ulk2*$^{+/-}$ pyramidal neurons.

To examine molecular underpinnings for the observed electrophysiological changes in *Ulk2*$^{+/-}$ neurons, levels of surface expression of the major excitatory and inhibitory neurotransmitter receptors [i.e. *N*-methyl-D-aspartate (NMDA) and gamma-aminobutyric acid $(GABA)_A$ receptors] were evaluated in cultured cortical neurons via biotinylation experiments. Both total and surface expression levels of the NMDA receptors were equivalent between WT and *Ulk2*$^{+/-}$ neurons (Fig. 2C and D). In contrast, levels of surface expression of $GABA_A$ receptors (α2 and α5 subunits) in *Ulk2*$^{+/-}$ neurons were lower than in WT, while the total levels of these receptors remained unchanged between the two genotypes (Fig. 2C and D).

Reducing the level of *p62* expression restores $GABA_A$ receptor surface presentation and rescues the behavioral deficits in *Ulk2*$^{+/-}$ mice

To address the role of p62 in the regulation of $GABA_A$ receptor surface expression, *Ulk2*$^{+/-}$ mice were bred with *p62*$^{+/-}$ mice, and the levels of $GABA_A$ receptor surface expression in primary cortical neurons of *Ulk2*$^{+/-}$; *p62*$^{+/-}$ mice were evaluated when compared with those in control or *Ulk2*$^{+/-}$ mice. Reducing *p62* gene dosage in *Ulk2*$^{+/-}$ neurons led to significant up-regulation of the $GABA_A$ receptor surface expression (Fig. 3A; Supplementary Material, Fig. S3A and B).

We next evaluated whether reducing *p62* gene dosage can rescue behavioral deficits in *Ulk2*$^{+/-}$ mice; PPI deficits were normalized to the levels equivalent to those in WT (Fig. 3B); cognitive inflexibility in the rule shifting assay was rescued (Fig. 3C and D). Thus, p62 not only serves as a marker for attenuated autophagy in neurons, but also plays a functional role in the regulation of $GABA_A$ receptor surface presentation, as well as behaviors.

Pharmacological intervention with rapamycin or its analog, CCI-779, is known to enhance autophagic processes and degrades p62 proteins (21,22). Indeed, we observed amelioration of the pathologically elevated p62 levels in *Ulk2*$^{+/-}$ mice with chronic treatment with CCI-779 (Fig. 1B). Importantly, the surface expression of $GABA_A$ receptors in *Ulk2*$^{+/-}$ cultures was normalized by rapamycin treatment (Fig. 2C and D). Furthermore, CCI-779 treatment normalized attenuated PPI (Fig. 1C and D) and cognitive inflexibility (Fig. 1F and G). These results support the notion that the observed phenotypes in *Ulk2*$^{+/-}$ mice are likely caused by attenuation of autophagic processes involving p62. Notably, PPI deficits in *Ulk2*$^{+/-}$ mice were not normalized by clozapine (Fig. 1C and D).

Interfering with p62–GABARAP interaction restores $GABA_A$ receptor surface presentation and rescues the behavioral deficits in *Ulk2*$^{+/-}$ mice

To further address the molecular mechanism by which the p62 dosage affects $GABA_A$ receptor surface presentation, we hypothesized that elevated p62 levels could titrate out proteins essential for $GABA_A$ receptor trafficking. p62 interacts with $GABA_A$ receptor-associated protein (GABARAP) (23), a scaffolding protein known to regulate $GABA_A$ receptor trafficking (24). Therefore, we reasoned that interfering with p62–GABARAP interaction could liberate GABARAP, leading to restoration of $GABA_A$ receptor surface presentation. Because ∼10-amino acid LIR (LC3-interacting region) motif located in the middle of the p62 protein was shown to bind GABARAP (23), we designed a 26-amino acid peptide (26aa-peptide) that encompasses this region, and tested its potential to interfere with p62–GABARAP interaction (Fig. 4A). When heterologously expressed in HEK293 cells, this 26aa-peptide inhibited p62–GABARAP interaction in a dose-dependent manner (Fig. 4A). Moreover, when the 26aa-peptide was transfected in *Ulk2*$^{+/-}$ primary cortical neurons, the level of cell surface $GABA_A$ receptor was upregulated, when compared with the neighboring non-transfected cells (Fig. 4A). We next investigated its effects on behavioral deficits in *Ulk2*$^{+/-}$ mice; introducing the 26aa-peptide via adeno-associated virus (AAV)-mediated delivery into the medial PFC significantly improved PPI deficits (Fig. 4B) and behavioral inflexibility (Fig. 4C and D). The results provide a proof of concept for the role of elevated p62 levels in sequestering GABARAP in *Ulk2*$^{+/-}$ mice.

p62 is elevated in olfactory neuronal cells in patients with sporadic cases of SZ and bipolar disorder

Given that cortical excitatory–inhibitory imbalance, PPI deficits and behavioral inflexibility are generally seen in patients with psychiatric conditions such as SZ and bipolar disorder (BP) (25,26), we questioned how the molecular signatures associated with attenuated autophagic processes could generally be seen as a neuronal trait associated with such psychiatric conditions. Although induced pluripotent stem cells-derived neurons are

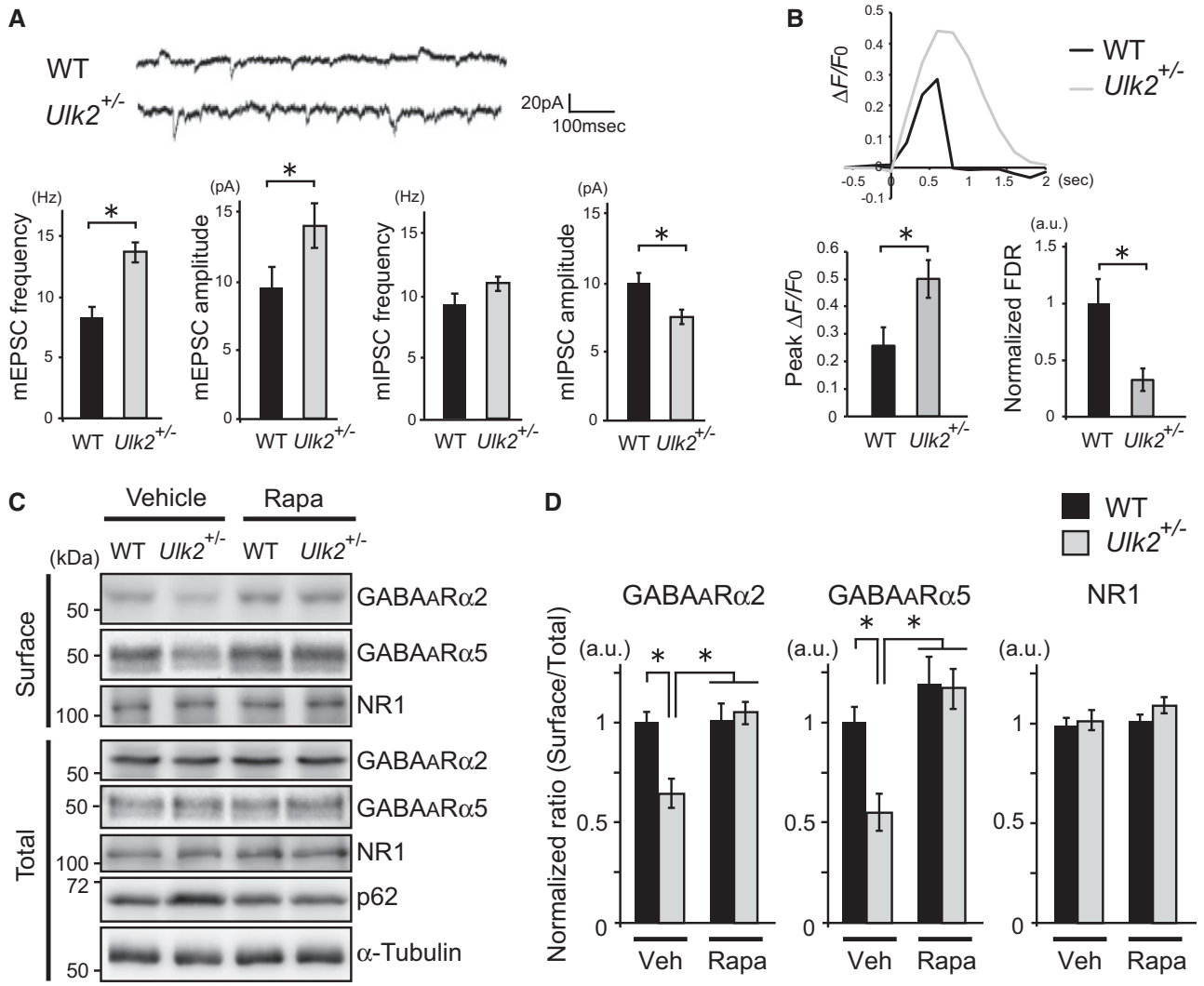

Figure 2. Reduced surface expression of $GABA_A$ receptors and imbalanced excitatory–inhibitory neurotransmission in *Ulk2*$^{+/-}$ pyramidal neurons. (**A**) Patch-clamp recording of miniature synaptic currents from WT and *Ulk2*$^{+/-}$ primary neurons (n =20 each) (16–25 DIV). Averages of mEPSC and mIPSC frequencies and amplitudes are plotted in the graph. *$P<0.05$ (Mann–Whitney test, two-tailed). (**B**) WT and *Ulk2*$^{+/-}$ primary cortical neurons were transfected with pCAG-GCaMP6, and $[Ca^{2+}]_i$ in each transfected neuron was measured following depolarization. Representative $[Ca^{2+}]_i$ changes ($\Delta F/F_0$) are plotted, and the averaged peak value and the FDR are shown in the graph (n =10 each). *$P<0.05$ (Mann–Whitney test, two-tailed). (**C, D**) Surface-biotinylated cell lysates from primary neurons cultured with or without rapamycin (100 nM, 30 min) were analyzed by western blot using anti-$GABA_A$ receptor α2 and α5 subunit and NR1 antibodies. Experiments were done in triplicate and densitometry analyses were done to evaluate the surface levels of each receptor by normalizing them against the total levels of respective receptor, and plotted in the graph. *$P<0.05$ (Kruskal–Wallis test).

useful for investigating specific disease variant-associated molecular changes, this labor-intensive and expensive experimental system is not practically optimal to address questions to sporadic or general cases. Instead, the use of surrogate tissues may be considered (27). Thus, we used olfactory neuronal cells obtained via nasal biopsy (28–30) and addressed the question with these cells from patients with sporadic cases of SZ and BP.

We examined levels of p62 and LC3 proteins in olfactory neuronal cells biopsied from sporadic cases of SZ and BP, when compared with the age, gender and race-matched healthy controls (Fig. 5A). p62 protein levels were significantly upregulated in cells derived from patients with SZ and BP (Fig. 5B; Supplementary Material, Fig. S4A and B). Furthermore, the ratio of LC3-II/LC3-I had a trend of upregulation, a sign of LC3-II accumulation and hence attenuated autophagy (Fig. 5C; Supplementary Material, Fig. S4A and B). Note that *p62* and *Lc3* mRNA levels showed no significant differences among groups (Fig. 5D). These results, in particular the de-coupling of the mRNA and protein levels, indicate that attenuated autophagic process is a cellular signature in neuronal cells from patients with sporadic SZ and BP.

Discussion

The present study demonstrates that the *Ulk2*-mediated process involving p62 regulation plays a critical role in higher brain functions, at least in part through maintenance of the excitatory–inhibitory balance in the PFC. The finding also suggests that neuronal autophagy regulates not only cellular viability but also homeostasis of brain functions, such as cognition. Although the CNV previously reported for *Ulk2* likely represents an extremely rare case among SZ, the underlying neurobiological deficit caused by *Ulk2* dysfunction (i.e. excitatory–inhibitory imbalance owing to elevated p62 expression) may provide a

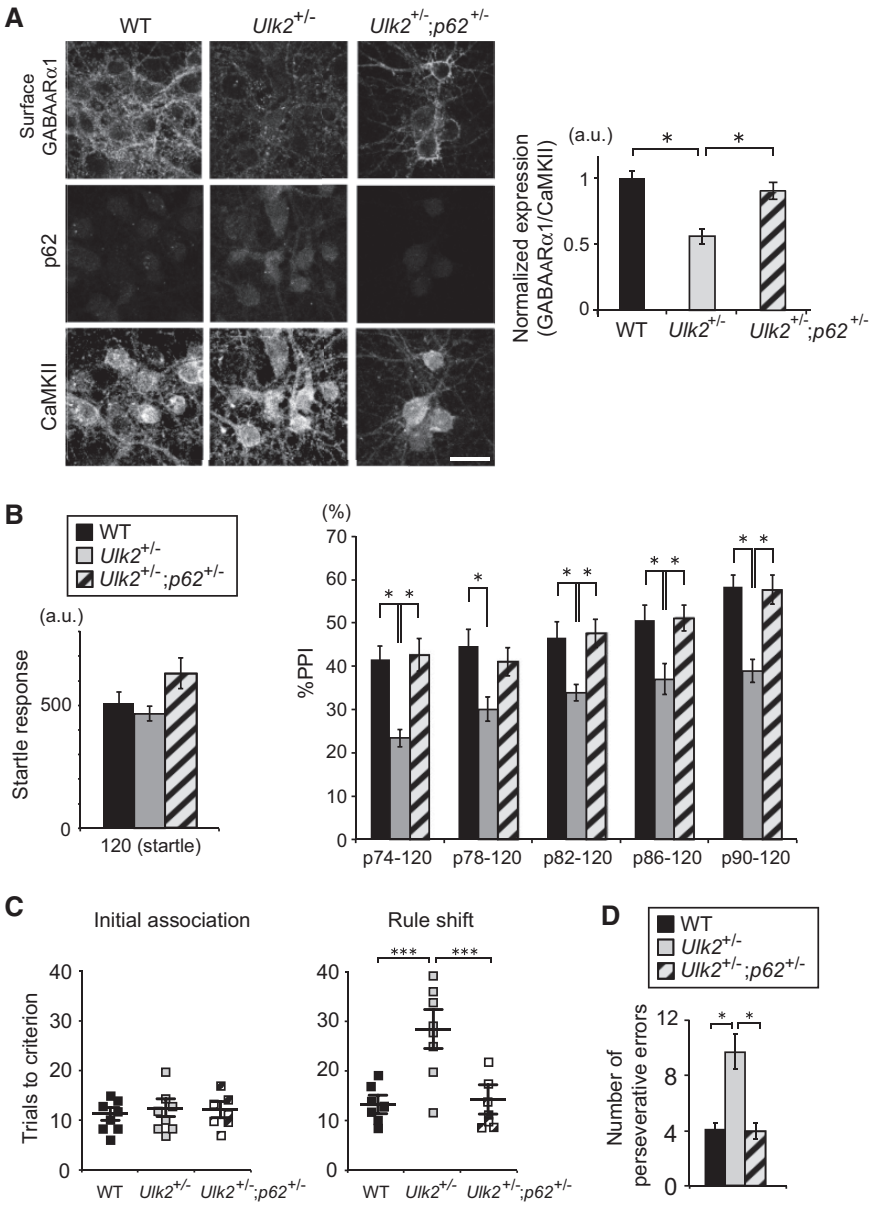

Figure 3. Reducing *p62* gene dosage rescues $GABA_A$ receptor surface presentation and behavioral deficits in $Ulk2^{+/-}$ mice. (**A**) Primary cortical neurons were prepared from mice with the indicated genotypes, and the cell surface staining was done at 16 DIV with anti-$GABA_A$ receptor α1 subunit antibody, followed by permeabilization and further staining with anti-CaMKII and p62 antibodies. Scale bar, 20 μm. Fluorescence intensities per soma were measured using ImageJ. *P< 0.05 (Kruskal–Wallis test). Lower magnification images are shown in Supplementary Material, Fig. S3A. (**B**) The amplitude of startle response (left) and %PPI (right) were evaluated for WT (n=9), $Ulk2^{+/-}$ (n=9) and $Ulk2^{+/-}$; $p62^{+/-}$ (n=12). Statistical significance in startle response [$F_{(2,\ 28)}$=5.548, P=0.0093] (one-way ANOVA) and in %PPI [$F_{(2,\ 28)}$=8.761, P=0.0011] (two-way ANOVA with repeated measures); *P <0.05, **P <0.01 (Bonferroni post hoc test). (**C**) Numbers of trials to criterion during the initial association phase, as well as the rule shift phase of the assays, were scored for WT (n=8), $Ulk2^{+/-}$ (n=8) and $Ulk2^{+/-}$; $p62^{+/-}$ (n=7). No significant difference during the initial association phase [$F_{(2,\ 20)}$=1.24, P=0.968]. Statistical significance during the rule-shift phase: $F_{(2,\ 20)}$=8.42, P<0.0001 (one-way ANOVA); ***P <0.001 (Bonferroni post hoc test). (**D**) Numbers of perseverative errors during the rule shift phase were scored. $F_{(2,\ 20)}$=5.27, P=0.038 (one-way ANOVA); *P <0.05 (Bonferroni post hoc test).

general pathophysiological mechanism pertinent to neuropsychiatric manifestation, including the sporadic cases of SZ.

Selective targeting of $GABA_A$ receptor by autophagy

Selective downmodulation of $GABA_A$ receptors on the surface of the pyramidal neuron likely leads to imbalanced excitatory–inhibitory neurotransmission in $Ulk2^{+/-}$ mice. How could neurons achieve such a selective regulation of a particular neurotransmitter receptor through autophagy? A previous study reported selective regulation of $GABA_A$ receptor surface presentation at the neuromuscular junction in *Caenorhabditis elegans*, in which $GABA_A$ receptors expressed on the muscle cells are selectively sorted via endocytosis from the postsynaptic membrane surface to traffic to the autophagosome upon denervation, whereas acetylcholine receptors in the same cell did not traffic to the autophagosome (31). This study suggests a role of autophagy in selective sorting of $GABA_A$ receptors responsible for attenuated inhibitory neurotransmission. At the mechanistic level, we showed that a specific interaction of p62 with GABARAP, which positively regulates endocytic turnover of $GABA_A$

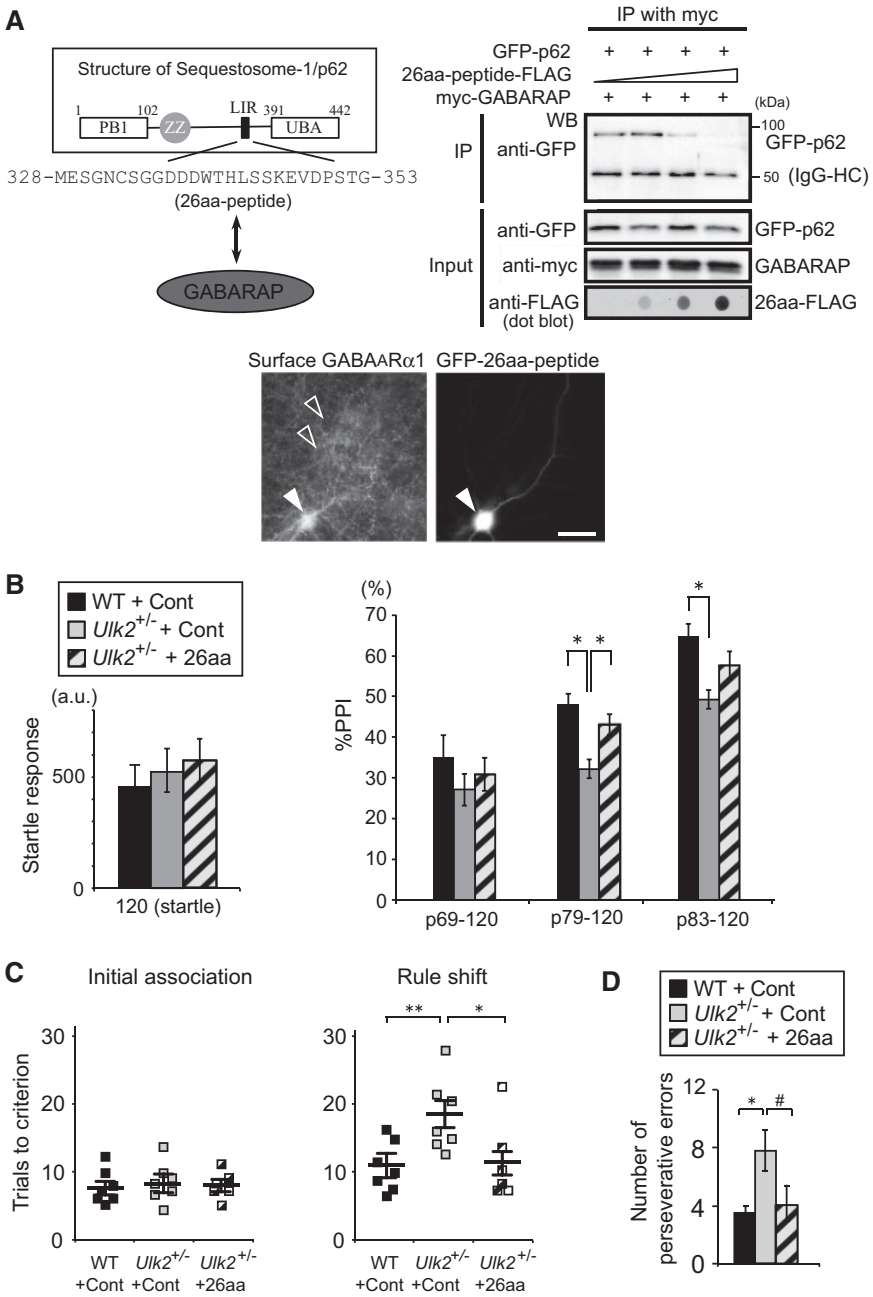

Figure 4. Interfering with p62–GABARAP interaction rescues $GABA_A$ receptor surface presentation and behavioral deficits in *Ulk2*$^{+/-}$ mice. (**A**) Schematic illustration of sequestosome-1/p62 protein structure and designing strategy for the 26-amino acid peptide that interferes with p62–GABARAP interaction. The LIR (LC3-interacting region) contains a DDDWxxL motif that was shown to interact with GABARAP (23). Primary cortical neurons prepared from *Ulk2*$^{+/-}$ mice were transfected at 16DIV with an expression plasmid encoding GFP-26aa-peptide, and the cell surface $GABA_A$ receptor (α1 subunit) was immuno-stained without cell permeabilization. White arrow indicates a cell transfected with GFP-26aa-peptide, and open arrows indicate neighboring non-transfected cells. Scale bar, 20 μm. (**B**) The amplitude of startle response (left) and %PPI (right) were evaluated for WT injected with control AAV (n=7), *Ulk2*$^{+/-}$ with control AAV (n=7), and *Ulk2*$^{+/-}$ with 26aa-peptide AAV (n=6). No significant difference in startle response [$F_{(2,\ 17)}$=1.045, P=0.833] (one-way ANOVA). Statistical significance for %PPI: $F_{(2,\ 17)}$=8.53, P =0.0126 (two-way ANOVA with repeated measures); *P <0.05 (Bonferroni post hoc test). (**C**) Numbers of trials to criterion during the initial association phase, as well as the rule shift phase of the assays, were scored for WT injected with control AAV (n=7), *Ulk2*$^{+/-}$ with control AAV (n =7), and *Ulk2*$^{+/-}$; *p62*$^{+/-}$ with 26aa-peptide AAV (n=6). *P <0.05, **P <0.01. No significant difference during the initial association phase [$F_{(2,\ 17)}$=1.02, P =0.827]. Statistical significance during the rule-shift phase: $F_{(2,\ 17)}$=7.74, P=0.018 (one-way ANOVA); *P <0.05, **P <0.01 (Bonferroni post hoc test). (**D**) Numbers of perseverative errors during the rule shift phase were scored. $F_{(2,\ 17)}$=4.58, P =0.046 (one-way ANOVA); *P <0.05, #P=0.057 (Bonferroni post hoc test).

receptors (24), may be important: elevated p62 expression in *Ulk2*$^{+/-}$ pyramidal neurons appears to sequester a higher proportion of GABARAP and limit the amount of GABARAP available for $GABA_A$ receptor surface presentation.

Linking the data from the animal model and patient neuronal cells

Although both *p62* and *Ulk2* are ubiquitously expressed in all cell types in every tissue tested (11,32), it is currently unknown

A

	Normal Control (NC)	Schizophrenia (SZ)	Bipolar disorder (BP)
N	22	23	19
Age	34.41 ± 2.53	36.17 ± 2.57	42.16 ± 2.47
Gender (M:F)	18:04	17:07	7:12 *
Race (AA/Cau/Asian/mix)	13/9/0/0	14/6/2/1	1/14/1/3 *

*$P < 0.05$, Fisher's exact test

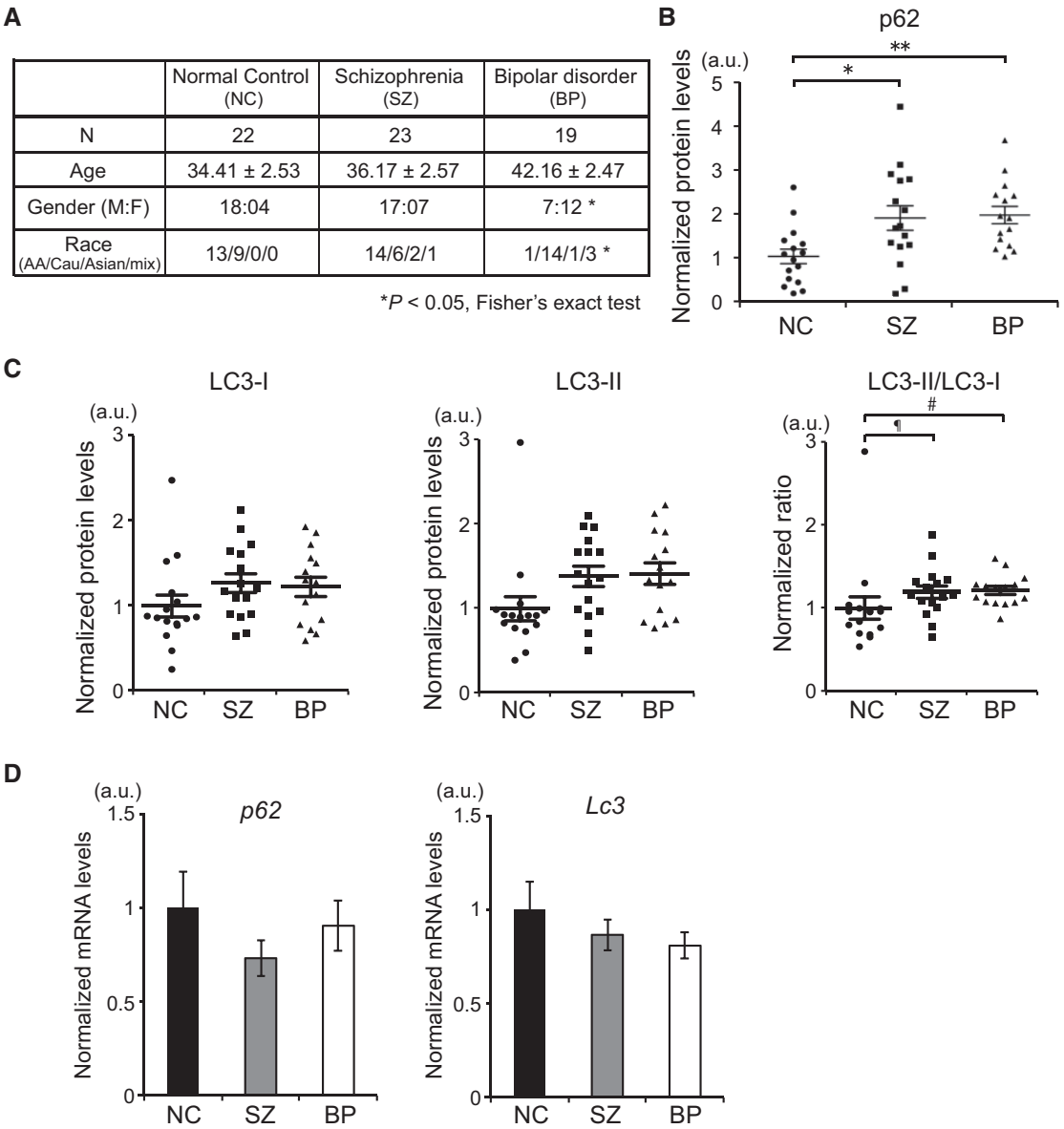

Figure 5. Attenuated autophagy in olfactory neuronal cells in sporadic cases of psychiatric disorders. (**A**) Demographics of human subjects in this study. *P <0.05 (Fisher's exact test). (**B**) The relative protein expression levels of p62 for each subject of control (circle), SZ (square) and BP (triangle) evaluated by western blot. *P<0.05, **P<0.01 (one-way ANOVA). See also Supplementary Material, Fig. S4A and B. (**C**) The relative protein expression levels of LC3-I, LC3-II and their ratio (LC3-II/LC3-I) for each subject of control (circle), SZ (square) and BP (triangle) evaluated by western blot. ¶P=0.067175, #P=0.054516. (**D**) qPCR analysis of *p62* and *Lc3* mRNA expression in control or patients-derived olfactory neuronal cells. No statistical significance (one-way ANOVA).

why p62 protein accumulation is predominantly observed in the pyramidal neurons of the PFC in *Ulk2*$^{+/-}$ mice. It is possible that the levels of autophagic activity necessary to maintain cellular homeostasis are differentially regulated via specific physiological demands determined by each cell type in a given tissue. Indeed, *Ulk1/Ulk2* double knockout mice show severer neuronal loss in the hippocampus than in the cerebellum (11). Nevertheless, in a pathological context, we observed attenuated autophagic activity even in olfactory neuronal cells from patients with sporadic SZ and BP. Thus, pathological deregulation of autophagic processes may occur in a cell type-preferential manner through combination of both intrinsic cellular vulnerability and circuit-wide physiological demands, thereby underlying sporadic psychiatric conditions. Furthermore, our data from an animal model suggests that deregulated autophagy may play a causal role in neuropsychiatric manifestations, rather than representing mere incidental or compensatory changes.

Translational potential of the present study

Although there are means of intervening with a type of clinical manifestations (e.g. positive symptoms) observed in patients with SZ, via the use of antipsychotics, the medications may not be effective to other critical symptoms, such as negative symptoms and cognitive dysfunction (33). Clozapine is known as the medication with superior efficacy to all other antipsychotics, but some patients show treatment resistance to clozapine even in positive symptoms. Thus, new therapeutic strategies different from clozapine and other antipsychotics are awaited. In the

present study, we observed that sensorimotor gating deficits and cognitive inflexibility in *Ulk2*$^{+/-}$ mice could be ameliorated when *p62* gene dosage was reduced or by reducing the levels of p62 protein using a rapamycin analogue CCI-779, but not with clozapine. We cautiously but optimistically interpret that p62-associated autophagic signaling cascade may be a potential target for drug development at least for SZ. In summary, the present study provides a novel concept that p62-associated autophagic signaling cascade may be an important pathophysiological mediator for sporadic cases of SZ and BP, by affecting the cortical excitatory–inhibitory balance and higher brain functions, such as sensorimotor gating and cognitive flexibility.

Materials and Methods

Animals

Conditional *Ulk2* knockout mice (*Ulk2tm1Thsn/J*) and transgenic mice that express EIIa-Cre, CaMKIIα-CreERT2, or Viaat-Cre were obtained from The Jackson Laboratory (Bar Harbor, USA). *Ulk2* heterozygous mice were generated as previously described (14). *p62* knockout mice were generated as described (32). Mice were maintained on the C57BL/6J genetic background for at least 12 generations. Eight- to 12-week old male mice were used for behavioral analysis. All behavioral experiments and data collection were performed by the experimenters who were blind to animal genotypes and identity of treatment conditions. Maintenance of mouse colonies and experiments using mice were in accordance with the NIH Guide for the Care and Use of Laboratory Animals, and approved by the Committee on Animal Research at Kyoto University Graduate School of Medicine.

Prepulse inhibition

The startle response and PPI were measured using a startle reflex measurement system (SR-LAB) as described (34), with minor modifications. The test session began by placing a male mouse in a plastic cylinder and leaving it undisturbed for 30 min. The background white noise level in the chamber was 70 dB. A prepulse–pulse trial started with a 50-ms null period, followed by a 20-ms prepulse white noise (74, 78, 82, 86, or 90 dB). After a 100-ms delay, the startle stimulus (a 40-ms, 120 dB white noise) was presented, followed by a 290-ms recording time. The total duration of each trial was 500 ms. A test session consisted of six trial types (pulse-only trial, and five types of prepulse–pulse trial). Six blocks of the six trial types were presented in a pseudorandomized order such that each trial type was presented once within a block. The formula 100− [(response on acoustic prepulse−pulse stimulus trials/startle response on pulse-only trials) ×100)] was used to calculate %PPI.

Rule shift assay

Cognitive flexibility was evaluated in the rule-shifting assay, essentially as described (19,20). In brief, mice were habituated to food, odor cues (i.e. coriander and garlic powder), texture cues (i.e. fine and coarse digging media), and feeding apparatus prior to testing, and then food-deprived a day before the assays. Mice were initially trained in a sequence of trials to associate a food reward with a specific stimulus (i.e. either an odor or a digging medium). A varying combination of stimulus and food reward was presented to mice per trial. Eight consecutive correct responses to the food reward were considered reaching criterion (i.e. successful establishment of association between the stimulus and the food reward), and the number of trials to reach criterion were scored for each mouse tested. Upon rule shifting (e.g. from an odor cue to a different texture cue to predict reward), numbers of errors owing to perseveration to an old rule were scored before reaching new criterion.

Drug delivery

CCI-779 was dissolved in phosphate-buffered saline (PBS) (pH 7.6) and injected daily (i.p., 10 mg/kg body weight) for 8–14 days. Clozapine was dissolved in PBS (pH 5.2) and injected daily (i.p., 1.5 mg/kg body weight) for 2 weeks. Tamoxifen (Sigma) was dissolved in corn oil (10 mg/ml) and injected daily (i.p., 1 mg/mouse) for five consecutive days.

Quantitative reverse transcription-polymerase chain reaction

Total RNA was extracted from PFC using RNeasy Mini kit (Qiagen), and reverse-transcribed with a ReverTra Ace cDNA synthesis kit (Toyobo). TaqMan probes were purchased from Applied Biosystems, Inc. (ABI). All data were normalized with *Gapdh* as reference.

Primary cortical neuron culture

Primary cortical neurons were prepared from E13.5 frontal cortex through papain treatment (0.5 μg/ml in Earle's balanced salt solution supplemented with 5 mM ethylenediaminetetraacetic acid (EDTA) and 200 μM L-cysteine), followed by mechanical trituration using fire-bore glass pipettes, and plated on poly-D-lysine-coated glass cover slips or glass-bottom dishes (MatTek). The cultures were recovered in serum-containing media [Neurobasal media supplemented with 10% horse serum, 5% fetal bovine serum and 2 mM glutamine (Gibco)] for 4 h and maintained in serum-free media [Neurobasal media supplemented with B-27 (1:50 diluted), 2 mM glutamine, 50 IU/ml penicillin and 50 μg/ml streptomycin], with half of media being replaced with fresh media every 2–3 days. The cultures were used for immunocytochemical analysis, surface biotinylation followed by western blot analysis, patch-clamp recording and Ca^{2+} imaging analysis as described below.

Immunohistochemistry and immunocytochemistry

For immunohistochemical analysis, brains of perfused mice ($n = 4$ per group) were serially cut into 50 μm-thick coronal sections using vibratome (VT1200S, Leica), and the sections from one cohort of mice (a littermate pair of wild-type and *Ulk2*$^{+/-}$ mice) were permeabilized in PBS containing 0.05% Triton X-100 for 1 h, and incubated for 30 min at room temperature in 10% goat serum (Chemicon) in PBS, and simultaneously immunostained for 16 h at 4°C with primary antibodies followed by Alexa Fluor® 488- or 546-conjugated secondary antibodies (Molecular Probes) for 1 h at room temperature. The stained samples were observed using a confocal microscope (SP8, Leica; 40× objective lens, NA =1.3); images of one optical section (1 μm thick) were acquired from three to six non-overlapping areas per section, randomly chosen in each brain region (PFC, visual cortex, nucleus accumbens, dorsolateral striatum, hippocampus, ventral tegmental area), and three to four serial sections were analyzed. The fluorescence intensities of p62 immunostaining were

measured from each neuronal soma (30–50 somas per section) using ImageJ (NIH), with the background levels of staining in adjacent regions being subtracted, and the average immunofluorescence intensity was calculated across all serial sections from every mouse used.

For immunocytochemical analysis, cultured primary neurons were fixed with 4% PFA in PBS for 15 min and permeabilized in PBS containing 0.05% Triton X-100 for 1 h. When the surface epitope was stained, the primary antibody was included in PBS containing 10% goat serum before permeabilization. The samples were incubated for 30 min at room temperature in 10% goat serum (Chemicon) in PBS, followed by primary antibodies for 16 h at 4°C and by secondary antibodies (Molecular Probes) for 1 h at room temperature.

The primary antibodies used were anti-p62 (guinea pig, 1:400, MBL), anti-CaMKIIα [mouse monoclonal (6G9), 1:500, Stressmarq], anti-GAD67 [mouse monoclonal (1G10.2), 1:1000, Chemicon], anti-$GABA_A$ receptor α1 subunit [rabbit, 1:500, Alomone labs; or mouse monoclonal (S95–35), 1:500, LSBio] and anti-ULK2 (rabbit, 1:50, Thermo).

Surface biotinylation and western blots

Biotinylation of cell surface proteins was performed in primary neuron cultures using the cell surface protein isolation kit (Pierce) according to the manufacturer's protocol. Briefly, cells were incubated with ice-cold PBS containing Sulfo-NHS-SS-Biotin (Pierce) for 30 min with gentle rocking at 4°C. Cells were then lysed and precipitated with NeutrAvidin beads. Precipitated proteins were eluted from the NeutrAvidin beads with loading buffer containing dithiothreitol and heated for 5 min at 95°C and then analyzed by western blot. The primary antibodies used were anti-$GABA_A$ receptor α2 subunit (rabbit, 1:1000, Abgent), anti-$GABA_A$ receptor α5 subunit (rabbit, 1:1000, R&D Systems), anti-NR1 [rabbit monoclonal (1.17.2.6), 1:1000, Millipore], anti-p62 (guinea pig, 1:1000, MBL), anti-α-tubulin [mouse monoclonal (B-5-1-2), 1:8000, Sigma] and anti-LC3B (rabbit, 1:1000, Novus).

Patch-clamp recording

Primary cortical neurons prepared as above were plated on poly-D-lysine-coated glass cover slips. Whole-cell clamp recordings were performed on the cultured neurons at 16–25 days *in vitro* (DIV) with EPC10 (HEKA) amplifier at room temperature. Fire-polished glass patch pipettes of 3–6 MΩ were used, and the membrane current was recorded at a holding potential of −50 mV. mEPSCs or mIPSCs larger than 4 pA were analyzed. The composition of the external saline was (in mM) 145 sodium chloride (NaCl), 5 potassium hydroxide (KOH), 10 4-(2-hydroxyethyl)-1-piperazineethanesulfonic acid (HEPES), 2 calcium chloride ($CaCl_2$), 1 magnesium chloride ($MgCl_2$) and 10 glucose, pH 7.3. The composition of the intracellular solution was 140 D-glucuronate, 155 KOH, 7 potassium chloride (KCl), 5 ethylene glycol-bis(β-aminoethyl ether)-*N*,*N*,*N*′,*N*′-tetraacetic acid and 10 HEPES, pH 7.3. The junction potential of 14 mV was corrected as in a previous study (35). Recorded neurons were fixed and stained with anti-CaMKIIα (1:500, Stressmarq) to confirm their identity as pyramidal neurons.

Ca^{2+} imaging in dissociated culture

Primary cortical neurons prepared from E13.5 frontal cortex as above were plated on poly-D-lysine-coated glass-bottom dishes (MatTek). Cells were transfected at 14–18 DIV with pCAG-GCaMP6m (36) using lipofectamine 2000 (Invitrogen), according to the standard protocol. Two days post-transfection, cells were depolarized by final concentration of KCl (25 mM) plus $CaCl_2$ (30 mM), and imaged with an IX81 fluorescence microscope (Olympus) equipped with an objective lens (UPlanSApo, N.A. 1.35, 60×, for oil, Olympus), a heated stage (37°C), an auto-injector for drug delivery, and a CoolSNAP CCD camera (HQ2, Photometrics). A series of images were acquired from soma and dendrites at 30 frames/s, for 5 s prior to and 25 s following depolarization, using MetaMorph (Molecular Devices). Relative changes in fluorescence ($\Delta F/F_0$) were calculated by normalizing the fluorescence intensity at a given time with the level of baseline fluorescence measured before the onset of depolarization. Peak values for $\Delta F/F_0$ were scored, and the fluorescence decay rate (FDR) within 0.2 s from the peak fluorescence time point was calculated using the following formula:

$$\text{Normalized FDR} = \frac{[\Delta F/F_{0(t=\text{peak})} - \Delta F/F_{0(t=\text{peak}+0.2)}]_{(\text{for Ulk2}^{+/-}}}{[\Delta F/F_{0(t=\text{peak})} - \Delta F/F_{0(t=\text{peak}+0.2)}]_{(\text{for WT}}}$$

Cultured neurons were fixed and stained with anti-CaMKIIα (1:500, Stressmarq) to confirm their identity.

AAV-mediated gene delivery

Injection of AAV9 encoding a cytomegalovirus promoter-driven green fluorescence protein (GFP)-26aa-peptide (~5×10^{12} gc/ml) into the medial PFC was performed in 8-week-old mice. Mice were anesthetized by isoflurane inhalation and stereotaxic surgery was performed according to the standard procedures. The coordinate of the injection site was 2.0 mm anterior and 0.5 mm lateral to bregma at a depth of 1.5 mm for the PFC. A total of 0.5 μl of purified virus was delivered on each hemisphere over a 3 min period. The infected mice were used for behavioral assessment 2–3 weeks after surgical operations.

Clinical subjects and nasal biopsy

Patients were recruited from the outpatient psychiatric clinics of the Johns Hopkins Medical Institutions. Diagnosis was performed according to criteria of the Diagnostic and Statistical Manual of Mental Disorders-5th Edition (DSM-5) (American Psychiatric Association). Subjects were excluded from the study if they had a history of traumatic brain injury with loss of consciousness for >1 h, a history of drug abuse within 6 months of the study, drug dependence within 12 months of the study or a history of untreated major medical illnesses. Olfactory epithelial neuron cultures were prepared as described (37). The study was approved by the Johns Hopkins Institutional Review Board, and all subjects gave written consent for their participation.

Statistical analysis

All data were represented as mean ±standard error of the mean (SEM) and were analyzed by Kruskal–Wallis test followed by Dunn's multiple comparison test, unless otherwise noted. Behavioral assay data were analyzed by one-way or two-way analysis of variance (ANOVA) followed by Bonferroni post hoc

test, using Prism statistics software (GraphPad). Statistical significance in figures: $^{*}P < 0.05$, $^{**}P < 0.01$, $^{***}P < 0.001$.

Supplementary Material

Supplementary Material is available at *HMG* online.

Acknowledgements

We thank Shuhei Ueda, Makiko Morita, Yuichiro Hayashi, Tom Macpherson, Hiroyuki Okuno, Yoshiaki Tagawa, and Yoji Nakamura for advice; and Ayumi Saka and Sayaka Mauchi for technical assistance.

Conflict of Interest statement. None declared.

Funding

This work was supported by grants from the National Iinstitutes of Health [MH-084018, MH-094268 Silvio O. Conte Center, MH-069853, MH-085226, MH-088753 and MH-092443 to A.Sa., MH105660 to K.I., A.Sa.]; Stanley, S-R and RUSK Foundations (to A.Sa.); NARSAD and Maryland Stem Cell Research Fund (to K.I., A.Sa.); Department of Defense/ Congressionally Directed Medical Research Program [W81XWH-11-1-0269 to T.T.]; Childrends Tumor Foundation-Drug Discovery Initiative (to T.T.); Japan Society of Promotion of Science [49170001 to T.Y., 24689015 to T.F., 25110717 and 15H04259 to T.Hir., 15H01285 and 16K01948 to T.S., 15H04275, 16H06568 and 16K14579 to T.Hik.]; Takeda Science Foundation, the Naito Foundation, the Kato Memorial Trust for Nambyo Research, and the International Cooperative Research Program of Institute for Protein Research at Osaka University [ICRa-17-13] (to T.Hik.); and partly supported by Takeda Pharmaceutical Co. Ltd.

References

1. Mizushima, N. and Komatsu, M. (2011) Autophagy: renovation of cells and tissues. *Cell*, **147**, 728–741.
2. Hara, T., Nakamura, K., Matsui, M., Yamamoto, A., Nakahara, Y., Suzuki-Migishima, R., Yokoyama, M., Mishima, K., Saito, I., Okano, H. and Mizushima, N. (2006) Suppression of basal autophagy in neural cells causes neurodegenerative disease in mice. *Nature*, **441**, 885–889.
3. Komatsu, M., Waguri, S., Chiba, T., Murata, S., Iwata, J., Tanida, I., Ueno, T., Koike, M., Uchiyama, Y., Kominami, E. and Tanaka, K. (2006) Loss of autophagy in the central nervous system causes neurodegeneration in mice. *Nature*, **441**, 880–884.
4. Komatsu, M., Wang, Q.J., Holstein, G.R., Friedrich, V.L., Jr, Iwata, J., Kominami, E., Chait, B.T., Tanaka, K. and Yue, Z. (2007) Essential role for autophagy protein Atg7 in the maintenance of axonal homeostasis and the prevention of axonal degeneration. *Proc. Natl. Acad. Sci. U.S.A.*, **104**, 14489–14494.
5. Toda, H., Mochizuki, H., Flores III, R., Josowitz, R., Krasieva, T.B., LaMorte, V.J., Suzuki, E., Gindhart, J.G., Furukubo-Tokunaga, K., and Tomoda, T. (2008) UNC-51/ATG1 kinase regulates axonal transport by mediating motor-cargo assembly. *Genes Dev.*, **22**, 3292–3307.
6. Wairkar, Y., Toda, H., Mochizuki, H., Furukubo-Tokunaga, K., Tomoda, T. and DiAntonio, A. (2009) Unc-51 controls active zone density and protein composition by downregulating ERK signaling. *J. Neurosci.*, **29**, 517–528.
7. Shen, W. and Ganetzky, B. (2009) Autophagy promotes synapse development in Drosophila. *J. Cell Biol.*, **187**, 71–79.
8. Mochizuki, H., Toda, H., Ando, M., Kurusu, M., Tomoda, T. and Furukubo-Tokunaga, K. (2011) UNC-51/ATG1 controls axonal and dendritic development via kinesin-mediated vesicle transport in the Drosophila brain. *PLoS One*, **6**, e19632.
9. Tomoda, T., Kim, J.-H., Zhan, C. and Hatten, M.E. (2004) Role of Unc51.1 and its binding partners in CNS axon outgrowth. *Genes Dev.*, **18**, 541–558.
10. Hernandez, D., Torres, C.A., Setlik, W., Cebrián, C., Mosharov, E.V., Tang, G., Cheng, H.C., Kholodilov, N., Yarygina, O., Burke, R.E., Gershon, M. and Sulzer, D. (2012) Regulation of presynaptic neurotransmission by macroautophagy. *Neuron*, **74**, 277–284.
11. Joo, J.H., Wang, B., Frankel, E., Ge, L., Xu, L., Iyengar, R., Li-Harms, X., Wright, C., Shaw, T.I., Lindsten, T. *et al.* (2016) The noncanonical role of ULK/ATG1 in ER-to-Golgi trafficking is essential for cellular homeostasis. *Mol. Cell*, **62**, 491–506.
12. Sumitomo, A., Ueta, K., Mauchi, S., Hirai, K., Horike, K., Hikida, T., Sakurai, T., Sawa, A. and Tomoda, T. (2017) Ulk1 protects against ethanol-induced neuronal stress and cognition-related behavioral deficits. *Neurosci. Res.*, **117**, 54–61.
13. Kundu, M., Lindsten, T., Yang, C.Y., Wu, J., Zhao, F., Zhang, J., Selak, M.A., Ney, P.A. and Thompson, C.B. (2008) Ulk1 plays a critical role in the autophagic clearance of mitochondria and ribosomes during reticulocyte maturation. *Blood*, **112**, 1493–1502.
14. Cheong, H., Lindsten, T., Wu, J., Lu, C. and Thompson, C.B. (2011) Ammonia-induced autophagy is independent of ULK1/ULK2 kinases. *Proc. Natl. Acad. Sci. U.S.A.*, **108**, 11121–11126.
15. Cheong, H., Wu, J., Gonzales, L.K., Guttentag, S.H., Thompson, C.B. and Lindsten, T. (2014) Analysis of a lung defect in autophagy-deficient mouse strains. *Autophagy*, **10**, 45–56.
16. Lang, B., Pu, J., Hunter, I., Liu, M., Martin-Granados, C., Reilly, T.J., Gao, G.D., Guan, Z.L., Li, W.D., Shi, Y.Y. *et al.* (2014) Recurrent deletions of ULK4 in schizophrenia: a gene crucial for neuritogenesis and neuronal motility. *J. Cell Sci.*, **127**, 630–640.
17. Swerdlow, N.R. and Geyer, M.A. (1998) Using an animal model of deficient sensorimotor gating to study the pathophysiology and new treatments of schizophrenia. *Schizophr. Bull.*, **24**, 285–301.
18. Kellendonk, C., Simpson, E.H. and Kandel, E.R. (2009) Modeling cognitive endophenotypes of schizophrenia in mice. *Trends Neurosci.*, **32**, 347–358.
19. Bissonette, G.B., Martins, G.J., Franz, T.M., Harper, E.S., Schoenbaum, G. and Powell, E.M. (2008) Double dissociation of the effects of medial and orbital prefrontal cortical lesions on attentional and affective shifts in mice. *J. Neurosci.*, **28**, 11124–11130.
20. Cho, K.K., Hoch, R., Lee, A.T., Patel, T., Rubenstein, J.L. and Sohal, V.S. (2015) Gamma rhythms link prefrontal interneuron dysfunction with cognitive inflexibility in *Dlx5/6*$^{+/-}$ mice. *Neuron*, **85**, 1332–1343.
21. Schmelzle, T. and Hall, M.N. (2000) TOR, a central controller of cell growth. *Cell*, **103**, 253–262.
22. Ravikumar, B., Vacher, C., Berger, Z., Davies, J.E., Luo, S., Oroz, L.G., Scaravilli, F., Easton, D.F., Duden, R., O'Kane, C.J. and Rubinsztein, D.C. (2004) Inhibition of mTOR induces

autophagy and reduces toxicity of polyglutamine expansions in fly and mouse models of Huntington disease. *Nat. Genet.*, **36**, 585–595.
23. Pankiv, S., Clausen, T.H., Lamark, T., Brech, A., Bruun, J.A., Outzen, H., Øvervatn, A., Bjørkøy, G. and Johansen, T. (2007) p62/SQSTM1 binds directly to Atg8/LC3 to facilitate degradation of ubiquitinated protein aggregates by autophagy. *J. Biol. Chem.*, **282**, 24131–24145.
24. Wang, H., Bedford, F.K., Brandon, N.J., Moss, S.J. and Olsen, R.W. (1999) GABA(A)-receptor-associated protein links GABA(A) receptors and the cytoskeleton. *Nature*, **397**, 69–72.
25. Perry, W., Minassian, A., Feifel, D. and Braff, D.L. (2001) Sensorimotor gating deficits in bipolar disorder patients with acute psychotic mania. *Biol. Psychiatry*, **50**, 418–424.
26. Green, M.F. (2006) Cognitive impairment and functional outcome in schizophrenia and bipolar disorder. *J. Clin. Psychiatry*, **67(Suppl)**, e12–e18; discussion 36–42.
27. Gamo, N.J. and Sawa, A. (2014) Human stem cells and surrogate tissues for basic and translational study of mental disorders. *Biol. Psychiatry*, **75**, 918–919.
28. English, J.A., Fan, Y., Föcking, M., Lopez, L.M., Hryniewiecka, M., Wynne, K., Dicker, P., Matigian, N., Cagney, G., Mackay-Sim, A. and Cotter, D.R. (2015) Reduced protein synthesis in schizophrenia patient-derived olfactory cells. *Transl. Psychiatry*, **5**, e663.
29. Lavoie, J., Gassó Astorga, P., Segal-Gavish, H., Wu, Y.C., Chung, Y., Cascella, N.G., Sawa, A. and Ishizuka, K. (2017) The olfactory neural epithelium as a tool in neuroscience. *Trends Mol. Med.*, **23**, 100–103.
30. Lavoie, J., Sawa, A. and Ishizuka, K. (2017) Application of olfactory tissue and its neural progenitors to schizophrenia and psychiatric research. *Curr. Opin. Psychiatry*, **30**, 176–183.
31. Rowland, A.M., Richmond, J.E., Olsen, J.G., Hall, D.H. and Bamber, B.A. (2006) Presynaptic terminals independently regulate synaptic clustering and autophagy of $GABA_A$ receptors in *Caenorhabditis elegans*. *J. Neurosci.*, **26**, 1711–1720.
32. Komatsu, M., Waguri, S., Koike, M., Sou, Y.S., Ueno, T., Hara, T., Mizushima, N., Iwata, J., Ezaki, J., Murata, S. *et al.* (2007) Homeostatic levels of p62 control cytoplasmic inclusion body formation in autophagy-deficient mice. *Cell*, **131**, 1149–1163.
33. Nucifora, F.C., Jr., Mihaljevic, M., Lee, B.J. and Sawa, A. (2017) Clozapine as a model for antipsychotic development. *Neurotherapeutics*, **14**, 750–761.
34. Takahashi, N., Sakurai, T., Bozdagi-Gunal, O., Dorr, N.P., Moy, J., Krug, L., Gama-Sosa, M., Elder, G.A., Koch, R.J., Walker, R.H. *et al.* (2011) Increased expression of receptor phosphotyrosine phosphatase-β/ζ is associated with molecular, cellular, behavioral and cognitive schizophrenia phenotypes. *Transl. Psychiatry*, **1**, e8.
35. Hirano, T. and Kasono, K. (1993) Spatial distribution of excitatory and inhibitory synapses on a Purkinje cell in a rat cerebellar culture. *J. Neurophysiol.*, **70**, 1316–1325.
36. Chen, T.W., Wardill, T.J., Sun, Y., Pulver, S.R., Renninger, S.L., Baohan, A., Schreiter, E.R., Kerr, R.A., Orger, M.B., Jayaraman, V. *et al.* (2013) Ultrasensitive fluorescent proteins for imaging neuronal activity. *Nature*, **499**, 295–300.
37. Kano, S., Colantuoni, C., Han, F., Zhou, Z., Yuan, Q., Wilson, A., Takayanagi, Y., Lee, Y., Rapoport, J., Eaton, W. *et al.* (2013) Genome-wide profiling of multiple histone methylations in olfactory cells: further implications for cellular susceptibility to oxidative stress in schizophrenia. *Mol. Psychiatry*, **18**, 740–742.